



Plasma dispersion effect based super-resolved imaging in silicon

HADAR PINHAS, OMER WAGNER, YOSSEF DANAN, MEIR DANINO, ZEEV
ZALEVSKY, AND MOSHE SINVANI*

Faculty of Engineering and the Nano-Technology Center, Bar-Ilan University, Ramat Gan 52900, Israel
*sinvanm@gmail.com

Abstract: We present here a new method for shaping a pulsed IR ($\lambda = 1550\text{nm}$) laser beam in silicon. The shaping is based on the plasma dispersion effect (PDE). The shaping is done by a second pulsed pump laser beam at 532nm (in either a Gaussian mode or a donut mode) which simultaneously and collinearly illuminates the silicon's surface with the IR beam. Following the PDE, and in proportion to its spatial intensity distribution, the 532nm laser beam shapes the point spread function (PSF) by controlling the lateral transmission of the IR probe beam. The use of this probe in a laser scanning microscope allows imaging and a wide range of contactless electrical measurements in silicon integrated circuits (IC) being under operation. We propose this shaping method to overcome the diffraction resolution limit in silicon microscopy on and deep under the silicon surface.

© 2018 Optical Society of America under the terms of the [OSA Open Access Publishing Agreement](#)

1. Introduction

In optical microscopy, the resolution that can be obtained is limited by the diffraction property of light. This diffraction limit was discovered in the 19th century [1–3] and it means that far field optical microscopes cannot show details smaller than half of the wavelength of the illuminating light. Over the years a great effort was invested to break the diffraction limit barrier and many methods were developed [4–7] for this purpose.

In the field of fluorescence microscopy a breakthrough that paved the way to real optical nanoscopy [8], was proposed by S. W. Hell and J. Wichmann in 1994 [9]. They proposed a new type of scanning fluorescence microscope capable of resolving 35 nm in the far field and named it STED microscopy. This method was approved experimentally in 1999 by T. A. Klar and S. W. Hell [10] where they demonstrated resolution of ~ 100 nm. Since then this technique, beside others in fluorescence microscopy [11–13], has been improved dramatically, where super resolution of ~ 20 nm was achieved in biological samples [13] and $\sim 5\text{nm}$ for fluorescent color centers in diamond crystal [14]. They exploited the typical characteristics of the fluorescent molecules. The molecules were excited by a pulsed laser beam focused on the sample with optimal Gaussian PSF. A second pulsed laser beam with a donut shape - the STED beam, functions by stimulating depleting fluorescence laterally around the center of the excitation beam spot on the sample, while leaving a center focal spot active to emit fluorescence. This sharpened the PSF of the excitation beam, while allowing spatial control of the emission from the sample, which leads to enhanced resolution. Some other methods were introduced as well such as photoactivated localization microscopy (PALM) [15] and as stochastic optical reconstruction microscopy (STORM) [16]. However, these super resolution methods apply for fluorescent materials only.

There are other methods proposed for nanoscopy, based on Probe-Pump technique where the pump is in a donut form that shapes the probe beam exploiting different physical mechanisms. Menon et al [17] demonstrated approach of realizing sub diffraction nanoscopy by adding to the surface to be imaged, a photochromic absorption modulated layer and by that they have properly exploited the wavelength selective chemistry of the photochromic layer to overcome the diffraction limit. This approach is applied only for surface samples, and more than that, it needs the addition of extra layer of the photochromic material. Also, the

photochromic material is sensitive to the heating by the laser beam which decreases the modulation depth of the shaped probe beam. Wang et al [18] demonstrated far-field imaging of non-fluorescent species with sub-diffraction resolution based on saturated transient absorption microscopy which can applied on semiconductors and materials with very small absorption saturation level. Also, it needs the scan of 3 collinear laser beams.

Other proposed methods use Gold-Nano Particles (GNP) for super-resolution that have to be added on the imaged surface, for instance a photo-thermal microscopy based on non-linear effect for super-resolution [19], or a method based on modifying the PSF due to scattering from a single nanoparticle due to saturation [20]. Another method that is based on GNP presented a method for modifying the PSF into a donut-like shape, through the utilization of the plasma dispersion effect (PDE) of silicon-coated gold nanoparticles [21]. However, all of these methods are contrast agents dependent.

There are theoretical investigations for schemes to obtain sub-diffraction limited resolution in coherent anti-Stokes Raman scattering (CARS) [22–24]. Tzang et al shows super-resolution in label-free photo-modulated reflectivity of thermal harmonics [25].

In this paper we propose a new probe-pump method for super-resolution nanoscopy based on PDE in silicon, with no need for extra agent. It may allow imaging on and deep under the silicon surface, depending on the pump wavelength and its pulse duration.

Optical microscopy plays an important role in imaging and probing techniques for contactless inspection and metrology of silicon ICs. The main tool in this technology is an IR laser beam acting as a contactless probe applied on the IC from its back side while allowing direct access to the active areas buried inside the silicon chip [26]. For this purpose the chip thinned from its back side and optically polished. The beam shaping is done in the silicon substrate, travel through the active area and reflected back from the metallic contacts covering the front side of the chip and to the detector.

There are many kinds of contactless measurements, besides imaging, that can be done by laser probe scanning microscopy, and we will introduce here few of them. According to the PDE, due to different concentration of free charge carriers (FCC) for the different features on the chip, a static image of the features inside the silicon chip can be extracted by the measure of the reflected laser beam while scanning over the chip from its backside. Also, the functionality of features on or inside the chip can be tested under operation on a laser voltage imaging (LVI) mode with scanning beam over the chip, or by the laser voltage probe (LVP) mode while the beam is focused on a single feature on the chip for individual contactless electrical tests. These methods are extensively used in the silicon industry in the developing process of ICs for failure analysis [27]. This technology can be used, also, for optical reading of nonvolatile memories on a chip [28–32] and for contactless probing of secret data on field programmable gate arrays [33]. The best achieved resolution in this kind of laser scanning microscopes is half of IR laser wavelength which is $\lambda = 1340/2 = 670$ nm and it can be improved by a factor of 3 to become ~ 200 nm by the adding of solid immersion lens (SIL) [34].

In this paper, we present a new method for shaping the PSF of IR laser beam in silicon which we name “Silicon Photonics STED” (SPS). By saying STED-like we did not refer to the fluorescence related physics of the stimulated emission depletion (STED) process. By saying STED-like we meant that the operation principle in respect to the super resolution aspect of the approach has direct similarity to STED. What we mean is that by using the plasma dispersion non-linearity of the silicon we generate a point spread function (PSF) having high spatial frequencies that may be much higher than the, diffraction limit half λ , and thus when such PSF scans the target (i.e. the PSF is multiplied by the spatial content of the target) we can down-convert those high spatial frequencies to low frequencies that can be imaged by the laser scanning microscope.

We expect by this method to improve resolution of IR probe well below 110 nm in silicon ICs, which it is the best achieved today by the use of green ($\lambda = 577$ nm, and NA = 3.1) laser

probe on very thinned ($\sim 1 \mu\text{m}$) back side of the chip and the use of appropriate SIL lens [35,36].

2. The concept

Our method is based upon the PDE in silicon. IR laser beam in silicon can be shaped by changing the silicon complex refractive index locally via another laser beam absorbed in the silicon which acts as a pump. This change is induced by the change in the FCC density in the silicon due to the absorbed pump beam. In this method, spatial frequencies higher than the ordinary diffraction limited Gaussian shape PSF frequencies are induced. It is important to note that the proposed mechanism is non-linear because the absorption coefficient for the probe is proportional to the power of the pump therefore the total absorption of the probe is exponentially related to the absorption coefficient according to the Beer-Lambert law. Thus, the intensity of the probe is exponentially dependent on the intensity of the pump. The result of this technique is the improvement in the PSF of the IR beam. The shaping of the IR beam PSF can be done in two modes. The first mode is to induce a hole in its center by applying a narrower Gaussian pump beam on its center [21], see Fig. 1(a). In this mode the resolution can easily be improved by factor higher then 3, which is the ratio of probe to pump wavelengths and improved further towards the sub-wavelength regime due to the non-linearity of the PDE. In this case the PSF has a shape requiring post processing (decoding) in order to reconstruct the super-resolved image. The second mode is to apply a donut shape pump beam to leave a narrow part on the center of the IR beam to pass through, and the rest of the beam blocked (Fig. 1(b)). In both modes the same absorption mechanism is involved. Therefore, we expect induce of high spatial frequencies in both modes which will be reflected in the nano scales. However, we will see later that the second mode has the advantage to determine the diameter of the inner hole of the donut by manipulation of the diffusion of the FCC. In this paper we will concentrate on the first mode. For the second mode we need a picosecond pump laser, we don't have at the moment, and will present preliminary results only.

In previous works [37–40] we developed an all-optical silicon slab modulator for temporal modulation of an IR laser probe beam by a second pulsed green laser beam as a pump. The pump laser was absorbed in the silicon and generated FCC that block the IR probe beam via the PDE. The ability to block IR beam in silicon by induced FCC absorption, temporally and spatially, gives the basis for super-resolution imaging method in silicon as proposed in this paper for the first time.

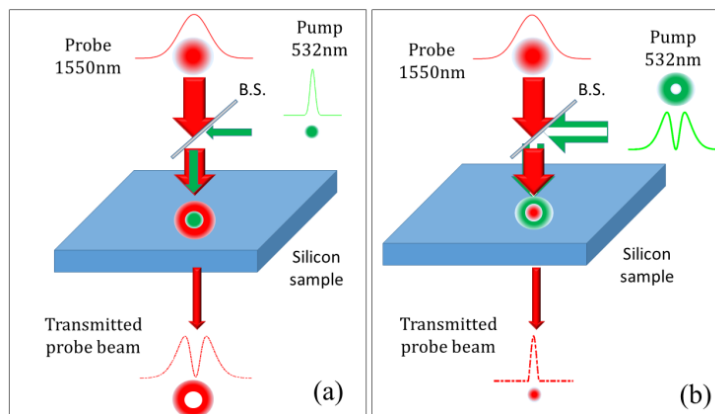


Fig. 1. Illustrations of the principle of the proposed two beam shaping methods. a) A narrow pump Gaussian beam at 532 nm, creates a hole in the middle of a wider IR beam. (b) Donut shape 532 nm pump beam blocks the periphery of the IR beam Gaussian and transmits a narrow beam in its center only.

3. Theory

As mentioned above, the physical mechanism we use for the modification of the silicon refractive index is the PDE, in which a change in the concentration of the FCC in the silicon modifies its complex refractive index. The complex refractive index may be written as $n = n + ik$ where the real part is the conventional index of refraction n . The imaginary part k is the optical extinction coefficient and it is related to the absorption coefficient α , by the Eq. $k = \alpha\lambda / 4\pi$. The PDE change of the real refractive index Δn , and the absorption coefficient, $\Delta\alpha$, can be predicted in good approximation by the free-carrier theory (Drude model) [41]. For c-Si and probe beam at wavelength $\lambda = 1550\text{ nm}$ Soref and Bennet [41,42] extracted empirical formulas for Δn and $\Delta\alpha(\text{cm}^{-1})$ as a function of the electron and holes concentration $\Delta N_e(\text{cm}^{-3})$ and $\Delta N_h(\text{cm}^{-3})$, respectively.

$$\Delta n = -8.8 \cdot 10^{-22} \cdot \Delta N_e - 8.5 \cdot 10^{-18} \cdot \Delta N_h^{0.8} \quad (1)$$

$$\Delta\alpha = 8.5 \cdot 10^{-18} \cdot \Delta N_e + 6.0 \cdot 10^{-18} \cdot \Delta N_h. \quad (2)$$

In our experiment the electron and holes concentration are generated by the pump laser beam where each photon creates an e-h pair. According to Eqs. (1) and (2) the increase in the FCC concentration causes a decrease in the real refractive index Δn , and an increase in the absorption $\Delta\alpha$, which blocks the IR beam in the silicon.

4. Experimental results

In Fig. 1(a) we present an illustration of the experiment we performed, as a proof of concept, for the proposed method. A silicon slab is illuminated by two pulsed diffraction limited Gaussian laser beams, a pump beam at wavelength of 532 nm and a probe beam at 1550 nm. The two beams are collinear and synchronized. The 532 nm beam width is narrower than the 1550 nm beam. The 532 nm beam is absorbed in the silicon and blocks the center of the 1550 nm beam to induce a hole in its center. The absorbed 532nm beam pulse generates FCC that causes a temporary change in the complex refractive index of the silicon due to PDE.

The change in the real and imaginary refractive index, as given in Eqs. (1) and (2), results in small phase and absorption changes. The sample we use is an intrinsic c-Si slab with resistivity $\rho > 1,000 \Omega\cdot\text{cm}$, 470 μm thick and area of $20 \times 20 \text{ mm}^2$, optically polished on both sides in parallel and without coating. Due to the high silicon's index of refraction, $n = 3.5$, it acts as a Fabry-Pérot (FP) resonator with spectral transmission (peak to valley) varying by factor of ~ 2 for the probe laser. The spectral transmission of the same sample taken with a scanning wavelength CW laser [38], shows peak to valley ratio of 3 as expected for uncoated silicon.

The experimental setup we use is shown in Fig. 2. The probe laser [43] is ~ 50 ps pulse width with jitter < 25 ps and beam diameter ($1/e^2$) of 1200 μm . The pump laser [44] is 17 ns pulse width with jitter < 4 ns and the beam focused to diameter of $\sim 30 \mu\text{m}$ on the silicon, as measured by a laser beam analyzer [45].

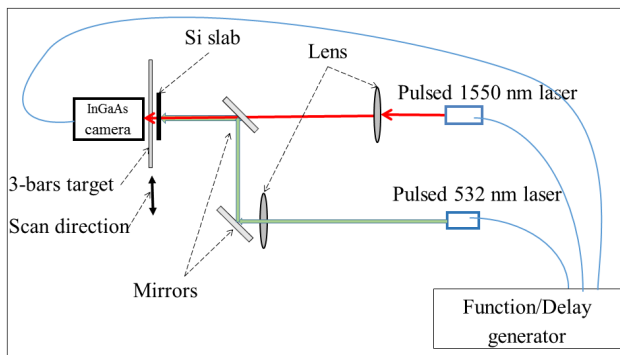


Fig. 2. The experimental setup.

The experiment was done where the probe and the pump lasers were focused on the silicon surface collinearly and pulsed simultaneously at a repetition rate of 10 pulses per second. The images of the transmitted probe laser beam were taken by InGaAs camera [46]. Image of the transmitted probe laser beam without the pump laser is given in Fig. 3(a). In Fig. 3(b) the probe is shown with the pump laser applied on its center demonstrating a beautiful dip in the center of the probe Gaussian beam.

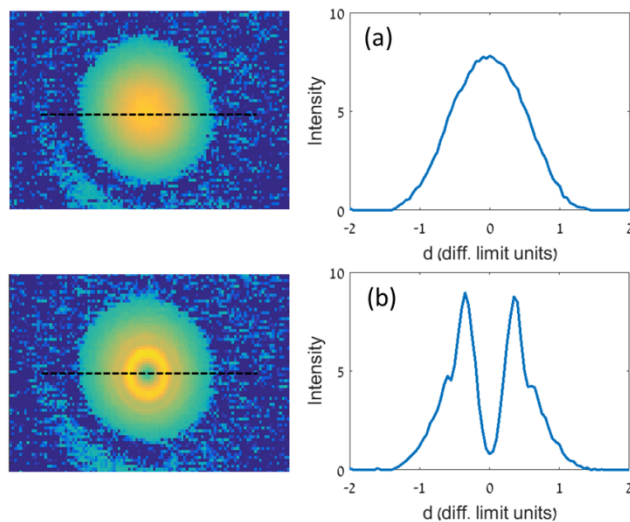


Fig. 3. The dip in the IR probe Gaussian beam induced by the green pump beam. (a) The image of the transmitted Gaussian probe beam with its profile. (b), the probe beam shaped by the pump beam superimposed on it to create a dip in its center (see [Visualization 1](#) for video that shows lateral and temporal behavior between probe and pump beams). One diffraction limit unit is $600 \mu\text{m}$.

In the attached visualization we show that the dip in the probe laser Gaussian beam appears only where the pump laser beam is co linear in space and synchronized with it in time. First, we move the pump laser beam in and out of the probe beam. Second, we change the delay time between the lasers pulses in steps of 10 ns and show that the effect completely disappeared in delay of 20 ns, even though the two lasers pulses are applied collinearly on the silicon continuously. In the video we can see also, how fast is the PDE in silicon where in the delay of 10ns the depth of the dip vibrates because of the jitter in the pump laser pulses.

In Fig. 4 we demonstrate the break of the diffraction limit, by the shaped beam of Fig. 3(b), in comparison with the unshaped beam of Fig. 3(a). The experiment was conducted on a

3-bars target, with a period of $500 \mu\text{m}$, scanned by the probe laser beam. The IR beam focused on Si surface with a very low NA (one diffraction limit unit is $600 \mu\text{m}$), and the camera was without a lens (see Fig. 2).

The experimental scan results of the 3-bars target using the unshaped beam are shown in Fig. 4(a), and for the shaped beam in Fig. 4(b). In both cases the raw scan is colored in red. Knowing the beam PSF we used MATLAB software to perform a standard Wiener filter algorithm [47] to DE-convolute the raw scan, and the results are colored in blue in both cases in Fig. 4. The scan with the unshaped probe beam, Fig. 4(a) shows unresolved pattern. On the other hand Fig. 4(b), shows clear resolution result of a scan with the shaped beam (the same beam shown in Fig. 3(b)). In this experiment the super resolution is demonstrated by the use of the shaped beam.

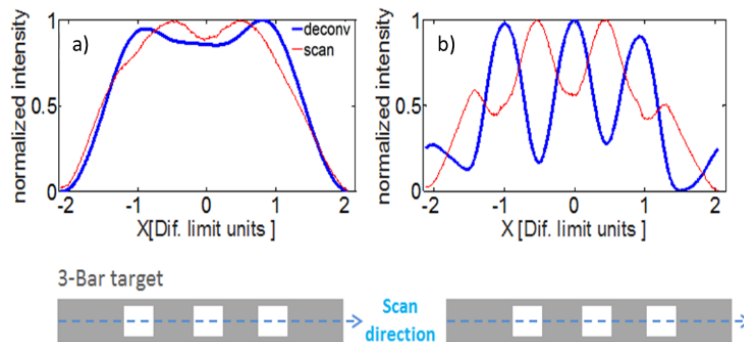


Fig. 4. Probe Gaussian IR laser beam at the diffraction limit scan across a 3-bars target (with a period of $500 \mu\text{m}$,) in two cases: (a). without the pump beam, as in Fig. 3(a), which shows unresolved target. The second case (b) is a scan of the target with the pump beam, with the dip in it, shows super-resolution where the target is well resolved. The red lines are the direct scan results and the blue lines are the direct scan results deconvoluted with the probe beam.

In Fig. 5 we, also, demonstrate the resolution enhancement in the spectral response of the shaped beam (red trace) compared with the unshaped (blue trace) probe beam. Where the shaped and the unshaped beams are shown in Fig. 5(a) and its Fourier transform (FT) are shown in Fig. 5(b).

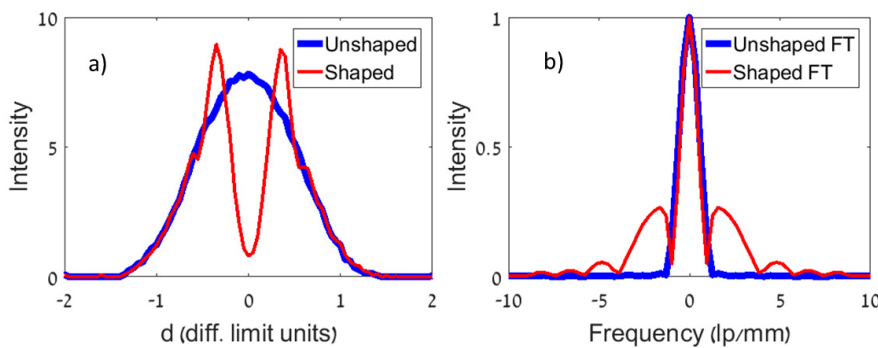


Fig. 5. The spectral response enhancement of the shaped probe beam compared to the unshaped beam.

As one can see in Fig. 3(b), the dip in the probe Gaussian is not complete and it reduces the sharpness of the 3-bars scan pattern. The shaped probe beam in Fig. 3(b) was taken by the camera without its lens; the transmitted probe beam was imaged on the camera's plan array detector directly from a distance of ~ 20 mm. However, when the camera with a zoom lens focused on the front surface of the silicon, at the point where the two beams are focused on,

we observe a full dip in the probe beam, as shown in Fig. 6(a), at pulse energy of 2.5 μJ . The dip depths as a function of the pump laser beam intensity are given in Fig. 6(b). The experimental results of the dips depth are shown in Fig. 6(a) where the black Gaussian is the probe beam only. The traces colored in - dark blue, light blue, purple, green and red attribute to the probe beam being superimposed with the pump beam pulses with energies of 0.2, 0.5, 1.25, 2.5, 5 μJ respectively. In Fig. 6(a) we show profile trace of 5 energy values out of 18 that were measured in the experiment. The dip depth at each energy measured from the bottom of the dip on each trace to the peak of the black Gaussian.

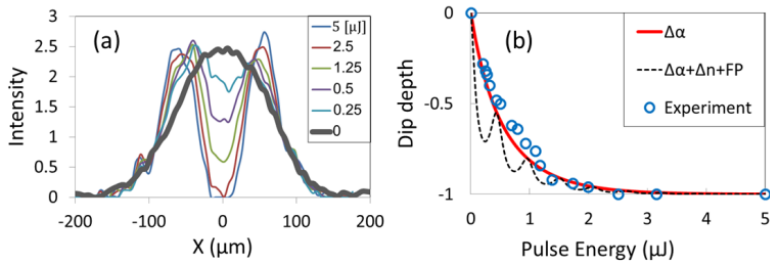


Fig. 6. The dip depth as a function of pump pulse energy. (a) - The profiles of the probe beam – without pump (black Gaussian) and with different 5 pump pulse intensities (the color traces). (b) - The dip depth as a function of the pump laser pulse energy – experimental (the blue circles), calculations via the PDE + FP (dashed black line), and calculation of FCC absorption only (red line).

The fit line in Fig. 6(b) is based on the following Eq. which includes the FB and the PDE:

$$\frac{I_{out}}{I_{in}} = \frac{(1-R)^2 e^{-(\Delta\alpha)d}}{(1-R e^{-(\Delta\alpha)d})^2 + 4R \cdot e^{-(\Delta\alpha)d} \cdot \sin^2\left(\frac{2\pi(n \cdot L + \Delta n \cdot d)}{\lambda}\right)}, \quad (3)$$

where R is the reflectivity of FP planes from both sides of the slab, $\Delta\alpha$ and n are the Si absorption coefficient and refractive index, respectively, λ is the probe wavelength, d is the absorption depth + diffusion length and L is the silicon sample thickness. The intensity of the pulse is introduced by $\Delta\alpha$ and Δn through the increase in the FCC density, derived by Eqs. (1) and (2).

5. Discussion

The dip depths in the probe beam as a function of the pump pulse energy are given in Fig. 6. The figure shows beautiful fit with the calculated values assuming FCC absorption, $\Delta\alpha$, only (the red line in Fig. 6(b)). The calculated dip depth values which are taking in account the dispersion Δn , the absorption $\Delta\alpha$, and the FP effect show an oscillatory behavior at lower pump intensity. But at higher pump intensities it converges to the absorption curve. These results indicate that for getting full modulation the physical dominant effect is indeed the FCC absorption $\Delta\alpha$. Therefore, the most important parameter for these calculations is the FCC concentration induced in the silicon by the pump pulse. The diameter of the pump beam on the silicon, as measured separately, was 30 μm . We have some uncertainty as for the size of the FCC volume induced by the pump beam because of the FCC diffusion [48–50]. For the 17 ns pulse duration of the pump beam, we assume diffusion of $\sim 10 \mu\text{m}$ for the FCC into the silicon. This value includes 1.3 μm for the penetration depth of the 532 nm pump photons, and 8 μm diffusion depth that was calculated for diffusion coefficient of $36\text{cm}^2/\text{s}$ for electrons in silicon during the 17 ns of the pump pulse. We assume that each photon that penetrates into the silicon creates $e\text{-}h$ pair. The $e\text{-}h$ pair recombination time is $>100 \text{ ns}$ [38,40] and it does not affect the FCC concentration during the pump pulse duration. For future work we plan to

overcome these uncertainties by the use of picosecond laser for the pump beam to reduce the FCC diffusion into the silicon.

The maximum flounce we used was 0.2 J/cm^2 which is lower by a factor of ~ 10 than the damage threshold for silicon [51]. Under the above assumptions, this flounce intensity for the pump beam creates FCC density of $\sim 10^{20} \text{ 1/cm}^3$.

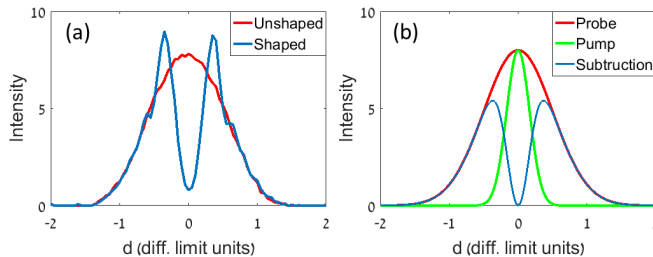


Fig. 7. Defocusing observed in the experiment compared to simple subtraction of a narrow Gaussian from a wider one. (a) The probe beam in the experiment, without the pump beam (red line) and with the pump beam (blue line). (b), Mathematical subtraction (blue line) of pump (green line) Gaussians from probe (red) Gaussian.

Another interesting effect we see is the defocusing. From Fig. 3(b) and Fig. 6(a) it can be seen that the rim of the dip in the shaped beam is brighter than the pick of the original probe Gaussian beam. This is not expected for a subtraction of two Gaussians as shown in Fig. 7(b). We attribute this effect to the defocusing [52–54] of the probe beam due to negative change in the index of refraction of the silicon due to the pump beam. The shape of the dip is governed by the Gaussian shape of the pump beam which creates on the silicon an area of Gaussian distribution of FCC in shape similar to the pump beam shape, i.e. high concentration in the center and lower in its periphery. Since the PDE is a nonlinear effect the block of the probe beam is significantly stronger in the center rather than on its periphery. However, the lower FCC concentration in the periphery still slightly reduces the silicon index of refraction and causes defocusing of the probe beam. Thus, another major novelty of this method is that we can get a focusing from this defocusing effect if we use a donut shape for the pump beam, instead of the Gaussian beam, as shown in Fig. 1(b). The usage of donut shape for the pump beam will resemble the STED method in laser scanning fluorescence nanoscopy.

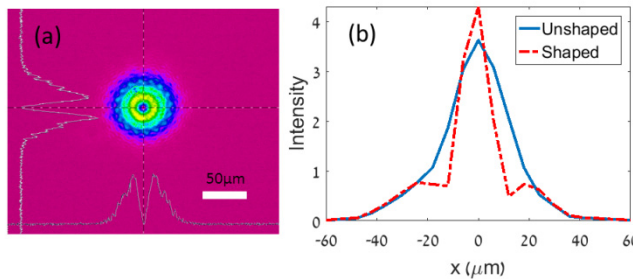


Fig. 8. ‘Silicon Photonics STED’: Preliminary experiment. (a) The donut shape pump beam. (b) The probe beam with (red dashed) and without (blue line) the donut pump on it.

In Fig. 8 we show preliminary experimental results for the shaping of the IR beam PSF by a donut shape for the pump beam. The donut shape for the pump beam was generated by spiral phase plate (Vortex plate) [55] inserted at the output of the pump laser. We see in Fig. 8(b) that the modulation depth of the shaped beam is not full, even for the pump pulse fluency we had. We tried to increase the flounce of the pump pulse by more focusing but because of the FCC diffusion toward the center of the donut at the pump pulse duration (17 ns), the IR shaped beam was blurred. We expect to overcome this problem by the use of a picosecond pump

laser, which we plan to acquire in the near future. Furthermore, the pulse temporal width of the pump laser may control the diffusion range of the FCC towards the center of the hole in the donut and to determine its diameter and by that even improve the high spatial frequencies that can be extracted in the proposed super resolving imaging process and to allow the improve in the resolution well below 100nm.

6. Conclusion

In this paper we have demonstrated a proof of concept for the SPS. We demonstrate the IR beam shaping by a second pump beam absorbed in the silicon via the PDE and show super resolution in silicon. This new method gives the ability to probe the silicon under surface in super resolution. It may serve as a very important tool in the field of nano electronics such as ICs failure analysis. It can also serve for detection of nano defects in silicon wafers, optical sensing of programmed charges in ICs and presumably it can be applied in other semiconductors. By the use of pump beam in longer wavelengths, closer to the absorption edge of the silicon, where the penetration depth of the pump beam can be increased up to ~100 μm under the silicon surface. The recombination time of photo-charges can also be measured precisely and directly by this method. We plan to continue this research, with picosecond pump laser, to get super resolution [21,56,57] well below the present limit of 100 nm, achieved in the microelectronics industry [34].

Acknowledgments

The authors would like to acknowledge Mr. Dov Friedman for assistance with the mechanical workshop.

References

1. É. Verdet, *Leçons D'optique Physique* (1869).
2. E. Abbe, "Beiträge zur Theorie des Mikroskops und der mikroskopischen Wahrnehmung," Arch. für Mikroskopische Anat. **9**(1), 413–418 (1873).
3. L. R. S. R. Rayleigh, "XV. On the theory of optical images, with special reference to the microscope," Philos. Mag. Ser. 5 **42**(255), 167–195 (1896).
4. S. Hell and E. H. K. Stelzer, "Fundamental improvement of resolution with a 4Pi-confocal fluorescence microscope using two-photon excitation," Opt. Commun. **93**(5-6), 277–282 (1992).
5. L. Schermelleh, R. Heintzmann, and H. Leonhardt, "A guide to super-resolution fluorescence microscopy," J. Cell Biol. **190**(2), 165–175 (2010).
6. M. Fernández-Suárez and A. Y. Ting, "Fluorescent probes for super-resolution imaging in living cells," Nat. Rev. Mol. Cell Biol. **9**(12), 929–943 (2008).
7. B. Huang, H. Babcock, and X. Zhuang, "Breaking the Diffraction Barrier: Super-Resolution Imaging of Cells," Cell **143**(7), 1047–1058 (2010).
8. S. W. Hell, "Far-field optical nanoscopy," Science **316**(5828), 1153–1158 (2007).
9. S. W. Hell and J. Wichmann, "Breaking the diffraction resolution limit by stimulated emission: stimulated-emission-depletion fluorescence microscopy," Opt. Lett. **19**(11), 780–782 (1994).
10. T. A. Klar and S. W. Hell, "Subdiffraction resolution in far-field fluorescence microscopy," Opt. Lett. **24**(14), 954–956 (1999).
11. M. Hofmann, C. Eggeling, S. Jakobs, and S. W. Hell, "Breaking the diffraction barrier in fluorescence microscopy at low light intensities by using reversibly photoswitchable proteins," Proc. Natl. Acad. Sci. U.S.A. **102**(49), 17565–17569 (2005).
12. M. G. L. Gustafsson, "Nonlinear structured-illumination microscopy: wide-field fluorescence imaging with theoretically unlimited resolution," Proc. Natl. Acad. Sci. U.S.A. **102**(37), 13081–13086 (2005).
13. S. W. Hell, "Microscopy and its focal switch," Nat. Methods **6**(1), 24–32 (2009).
14. E. Rittweger, K. Y. Han, S. E. Irvine, C. Eggeling, and S. W. Hell, "STED microscopy reveals crystal colour centres with nanometric resolution," Nat. Photonics **3**(3), 144–147 (2009).
15. E. Betzig, J. K. Trautman, T. D. Harris, J. S. Weiner, and R. L. Kostelak, "Breaking the diffraction barrier: optical microscopy on a nanometric scale," Science **251**(5000), 1468–1470 (1991).
16. M. J. Rust, M. Bates, and X. Zhuang, "Sub-diffraction-limit imaging by stochastic optical reconstruction microscopy (STORM)," Nat. Methods **3**(10), 793–796 (2006).
17. H.-Y. Tsai, S. W. Thomas 3rd, and R. Menon, "Parallel scanning-optical nanoscopy with optically confined probes," Opt. Express **18**(15), 16014–16024 (2010).
18. P. Wang, M. N. Slipchenko, J. Mitchell, C. Yang, E. O. Potma, X. Xu, and J.-X. Cheng, "Far-field imaging of non-fluorescent species with subdiffraction resolution," Nat. Photonics **7**(6), 449–453 (2013).

19. D. A. Nedosekin, E. I. Galanzha, E. Dervishi, A. S. Biris, and V. P. Zharov, "Super-Resolution Nonlinear Photothermal Microscopy," *Small* **10**(1), 135–142 (2014).
20. S.-W. Chu, T.-Y. Su, R. Oketani, Y.-T. Huang, H.-Y. Wu, Y. Yonemaru, M. Yamanaka, H. Lee, G.-Y. Zhuo, M.-Y. Lee, S. Kawata, and K. Fujita, "Measurement of a Saturated Emission of Optical Radiation from Gold Nanoparticles: Application to an Ultrahigh Resolution Microscope," *Phys. Rev. Lett.* **112**(1), 017402 (2014).
21. Y. Danan, T. Illovitsch, Y. Ramon, D. Malka, D. Liu, and Z. Zalevsky, "Silicon-coated gold nanoparticles nanoscopy," *J. Nanophotonics* **10**(3), 036015 (2016).
22. C. Cleff, P. Groß, C. Fallnich, H. L. Offerhaus, J. L. Herek, K. Kruse, W. P. Beeker, C. J. Lee, and K.-J. Boller, "Ground-state depletion for subdiffraction-limited spatial resolution in coherent anti-Stokes Raman scattering microscopy," *Phys. Rev. A* **86**(2), 023825 (2012).
23. W. P. Beeker, P. Gross, C. J. Lee, C. Cleff, H. L. Offerhaus, C. Fallnich, J. L. Herek, and K.-J. Boller, "A route to sub-diffraction-limited CARS Microscopy," *Opt. Express* **17**(25), 22632–22638 (2009).
24. V. Raghunathan and E. O. Potma, "Multiplicative and subtractive focal volume engineering in coherent Raman microscopy," *J. Opt. Soc. Am. A* **27**(11), 2365–2374 (2010).
25. O. Tzang, A. Pevzner, R. E. Marvel, R. F. Haglund, and O. Cheshnovsky, "Super-Resolution in Label-Free Photomodulated Reflectivity," *Nano Lett.* **15**(2), 1362–1367 (2015).
26. S. K. Garth, Y. H. Chen, and A. E. Stephens, "Effects of Dislocation and Bulk Micro Defects on Device Leakage," SEMICON Taiwan (2001).
27. C. Boit, R. Schlangen, A. Glowacki, U. Kindereit, T. Kiyan, U. Kerst, T. Lundquist, S. Kasapi, and H. Suzuki, "Physical IC debug – backside approach and nanoscale challenge," *Adv. Radio Sci.* **6**, 265–272 (2008).
28. L. Bidani, O. Baharav, M. Sinvani, and Z. Zalevsky, "Usage of Laser Timing Probe for Sensing of Programmed Charges in EEPROM Devices," *IEEE Trans. Device Mater. Reliab.* **14**(1), 304–310 (2014).
29. L. S. Koh, H. Marks, L. K. Ross, C. M. Chua, and J. C. Phang, "Laser Timing Probe with Frequency Mapping for Locating Signal Maxima," in 35th International Symposium for Testing and Failure Analysis (2009), pp. 33–37.
30. H. K. Heinrich, D. M. Bloom, and B. R. Hemenway, "Noninvasive sheet charge density probe for integrated silicon devices," *Appl. Phys. Lett.* **48**(16), 1066–1068 (1986).
31. S. Sayil, D. Kerns, and S. Kerns, "All-silicon optical contactless testing of integrated circuits," *Int. J. Electron.* **89**(7), 537–547 (2002).
32. C. Boit, H. Lohrke, P. Scholz, A. Beyreuther, U. Kerst, and Y. Iwaki, "Contactless visible light probing for nanoscale ICs through 10 μm bulk silicon," in *Proceedings of the 35th Annual NANO Testing Symposium (NANOTS2015)* (2015), pp. 215–221.
33. H. Lohrke, S. Tajik, C. Boit, and J. P. Seifert, *No Place to Hide: Contactless Probing of Secret Data on FPGAs* (2016).
34. "Private communication, Intel Inc. R&D center, Haifa, Israel," Priv. Commun. Intel Inc. R&D center, Haifa, Isr. (n.d.).
35. "<https://www.fei.com/products/efa/meridian-v-for-semiconductors/>," (n.d.).
36. "<http://checkpointtechnologies.com/products/#infrascan-ltm>," (n.d.).
37. H. Pinhas, L. Bidani, O. Baharav, M. Sinvani, M. Danino, and Z. Zalevsky, "All optical modulator based on silicon resonator," in *SPIE* (2015), **9609**, p. 96090L.
38. H. Pinhas, Y. Danan, M. Sinvani, M. Danino, and Z. Zalevsky, "Experimental characterization towards an in-fibre integrated silicon slab based all-optical modulator," *J. Eur. Opt. Soc. Publ.* **13**(1), 3 (2017).
39. R. Aharoni, M. Sinvani, O. Baharav, M. Azoulai, and Z. Zalevsky, "Experimental Characterization of Photonic Fiber-Integrated Modulator," *Open Opt. J.* **5**(1), 40–45 (2011).
40. R. Aharoni, O. Baharav, L. Bidani, M. Sinvani, D. Elbaz, and Z. Zalevsky, "All-optical silicon simplified passive modulation," *J. Eur. Opt. Soc.* **7**, 12029 (2012).
41. R. A. Soref and B. R. Bennett, "Electrooptical effects in silicon," *IEEE J. Quantum Electron.* **23**(1), 123–129 (1987).
42. G. T. Reed, *Silicon Photonics: The State of the Art* (John Wiley & Sons, 2008).
43. "Alphalas PLDD-20M 1550nm pulsed laser (Goettingen Germany, <http://www.alphalas.com/>)," (n.d.).
44. "Crystalaser QL532-025 532nm pulsed laser (Reno,Nevada, United States, <http://crystalaser.com/>)," (n.d.).
45. "Ophir SP620U Laser beam analyzer (Jerusalem, Israel, <http://www.ophiropt.com/>)," (n.d.).
46. "FLIR SC2500 InGaAs camera (Wilsonville, Oregon, United States, <http://www.flir.eu/home/>)," (n.d.).
47. W. Y. Lo and S. M. Puchalski, "Digital image processing," *Vet. Radiol. Ultrasound* **49**(1), S42–S47 (2008).
48. M. S. Tyagi and R. Van Overstraeten, "Minority carrier recombination in heavily-doped silicon," *Solid-State Electron.* **26**(6), 577–597 (1983).
49. D. Alamo and R. M. Swanson, "Modelling of minority-carriers transport in heavily doped silicon emitters," *Solid State Electronics* **30**, 1127 (1987).
50. C. Canali, C. Jacoboni, F. Nava, G. Ottaviani, and A. Alberigi-Quaranta, "Electron drift velocity in silicon," *Phys. Rev. B* **12**(6), 2265–2284 (1975).
51. X. Wang, Z. H. Shen, J. Lu, and X. W. Ni, "Laser-induced damage threshold of silicon in millisecond, nanosecond, and picosecond regimes," *J. Appl. Phys.* **108**(3), 033103 (2010).
52. C. Jun and H.-J. Eichler, "Laser Beam Defocusing at 1.06 gm by Carrier Excitation in Silicon," *Appl. Phys. B* **45**(3), 121–124 (1988).
53. T. Auguste, P. Monot, L.-A. Lompré, G. Mainfray, and C. Manus, "Defocusing effects of a picosecond terawatt

- laser pulse in an underdense plasma," Opt. Commun. **89**(2-4), 145–148 (1992).
54. V. V. Kononenko, E. V. Zavedeev, and V. M. Gololobov, "The effect of light-induced plasma on propagation of intense fs laser radiation in c-Si," Appl. Phys., A Mater. Sci. Process. **122**(4), 293 (2016).
 55. Holo-OR VL-209-Q-Y-A Vortex Lens - spiral phase plate (Ness Ziona, Israel,
http://www.holoor.co.il/Diffractive_Optics_Products/Diffractive_Vortex_Lens/Vortex-lens.php)
 56. Z. Zalevsky, D. Mendlovic, and A. W. Lohmann, "Optical systems with improved resolving power," Prog. Opt. **40**, 271–341 (2000).
 57. Z. Zalevsky and D. Mendlovic, *Optical Superresolution* (Springer, 2004).